ARTICLE

Nano-structured anti-biofilm surface widens efficacy against spindle-shaped and chain forming rod-like bacteria

Received 00th January 20xx,
Accepted 00th January 20xx

DOI: 10.1039/x0xx00000x

Xin Li [a,b^], Kwong-Hoi Tsui [c,d^], James K.H. Tsoi [d], David W. Green [d], Xiao-zhuang Jin [d], Yong Qiang Deng [b], Yao Min Zhu [b], Xu Guang Li [b], Zhiyong Fan [c], Gary Shun-pan Cheung [a*]

Current control of pathogenic bacteria at all biomaterial interfaces is poorly attuned to a broad range of disease-causing pathogens. Leading antimicrobial surface functionalization strategies with AMP's, Defensins, have not shown their promised efficacy. One of the main problems is lack of stability and swift clearance from the surface. Surface nanotopography bearing sharp protrusions is a non-chemical solution that is intrinsically stable and long-lasting. Previously, geometrically ordered arrays of nanotipped spines repel or rapidly rupture bacteria that come into contact. The killing properties so far work on cocci and rod-like bacteria, but there is no validation of the efficacy of protrusional surfaces on pathogenic bacteria with *** size and morphologies, thus broadening the utility of such surfaces to cover increasingly more disease entities. Here we report on a synthetic analogue of the nanotipped spines with pyrimadal shape that show great effectiveness on species of bacteria with strongly contrasting shapes and sizes. To highlight this phenomena in the field of dental applications where selective bacterial control is vital to the clinical success of biomaterial functions we textured PMMA against *Streptococcus mutans*, *Enterococcus faecalis*, *Porphyromonas gingivalis* and *Fusobacterium nucleatum*. These nanopyramid performed effectively at levels well above normal and roughened PMMA biomaterials for dentistry and a model material for general use in medicine and disease transmission in hospital environments.

Introduction

Biofilms are an immobilized community of microorganisms with a propensity to adhere to an extensive range of natural, inanimate, and synthetic surfaces [3]. The biofilm populates through a kaleidoscopic consortium of bacteria, fungi, amoeba, which cross-feed one another. The make-up of this microbial ecology is assembled within a concreted framework that provides incredible resilience. Biofilms are significant contaminants of engineering structures and among industrial processes, as well as medical materials. Most notably, they interfere and degrade the function of pipes and marine structures. Medical biofilms are a leading cause of 10% of all hospital-based infections and the leading cause of implant failures worldwide. In the US, 100,000 people die from persistent biofilm infections. Estimates put 80% of total chronic microbial infections as a biofilm. [1]

Microbial biofilms evolved tenacious adaptations for invasion and colonization onto inorganic, inanimate surfaces in contact with water, biomaterials, and tissues aided by some identifiable surface features, such as microstructure and charge, encouraging and supporting attachment and growth. In the body, the biofilm antagonizes the host's immunity into lengthening persistence and virulence.

Examples of antagonism as an evolved strategy include the inflammatory reactions of the gingiva to the accumulation of dental plaque, a unique type of biofilm, that is adherent to the root surface of teeth [2], along with the linings of endothelial and epithelial tracts and ducts or medical/dental implant failure [3]; denture-induced stomatitis [4]; and infections of the ceramic prosthesis [5], hip joints [6], bone cement [7, 8] contact lenses and intraocular lens [9]. Artificial medical devices, sutures, and catheters, routinely used in surgery and hospitals, respectively, are highly susceptible to microbial contamination, population, and biofilm formation [10]. Preventing biofilms from forming across medical and healthcare niches is vital around materials that come into contact with blood and tissues. Medical biomaterials are diverse. Polymers are particularly common materials for medical applications.

PMMA is in widespread use in many medical and dental appliances [11]. Given the water sorption ability and surface irregularities of PMMA after fabrication, bacteria can readily colonize on its surface [12]. The material itself may become weakened [13]. The oral cavity is the most microbial polluted environment in the human body, such that more than 600 different species of bacteria and over 100 million bacterial cells discovered in every milliliter of saliva [14]. A fraction of this number is potential pathogens or existing ones. Once biofilms establish themselves as an adherent coating at the surface, they are exceedingly difficult to remove by any chemical and physical means.

For instance, biofilms exposed to chlorine for 60 minutes can still contain living cells, and individual cells within a biofilm can persist in an iodine solution for up to 15 minutes [15]. Any antimicrobial agents

[a.] *Address here.*
[b.] *Address here.*
[c.] *Address here.*
† Footnotes relating to the title and/or authors should appear here.
Electronic Supplementary Information (ESI) available: [details of any supplementary information available should be included here]. See DOI: 10.1039/x0xx00000x

must be able to effectively penetrate the biofilm matrix (of exopolysaccharides) before they may act on the bacterial cells inside. Typically, increased amounts of an antibiotic or chemical agent are required. In medical facilities, large quantities of antiseptics and disinfectants control microbial contaminations. However, the use of antibiotics and chemical agents is prone to the development of resistance by bacteria, as well as adverse effects on patients. Indeed, antibiotics are becoming increasingly less effective, as many bacteria have developed antibiotic resistance [16]. Also, the desired or functional properties of the materials may be negatively affected [17]. Some chemicals might not be biocompatible or, even, exhibit toxicity, i.e., not safe for use on humans [18, 19], and hence should not be used as additives in PMMA. Physical disruption of the bacterial biofilm may work on the PMMA surface but only to varying degrees [20].

Modifying the surfaces of medical biomaterials in specific forms at microscale and nanoscale effectively reduces microbial accumulation. Surface modification interferes, in some cases, one part in the sequence of biofilm formation, and due to its experimental success, it is now a popular strategy [21]. Surface modification is a cosmetic augmentation of the material and does not affect the bulk properties. Since cells acutely respond to nanoscale features, there are approaches harnessing surface nanostructures to control all microbial attachment and growth. These small structures range amongst nano-protrusions (spikes and spines), nanopillars, nano-mounds, and nano-valleys. Interplay between nanostructures and microbes determines the attachment probabilities, the strength of adherence and organisation as well as the possibilities for colonization.

The size, shape, and pattern of the surface nanostructure are factors that might alter its antibacterial efficacy [22]. Surface protrusions with high aspect ratios, sharp edges and tight packing are in focus. Biophysical approaches to control bacteria are promising because there is low probability for emerging adaptations defying the laws of physics [23-27]. The trade-offs involved in developing a cell wall with equivalent stiffness to the material is highly unresolvable.

Theoretically, bacterial repellent surfaces can prevent biofilm formation and biofilm-mediated diseases without the need for any chemical agents already with provable efficaciousness and longstanding track record of killing microorganisms. In contrast to physical processes of kiliing bacteria toxic chemicals can be adapted to over many generations. Two main biophysical mechanisms are at play between surfaces protrusions and colonising bacteria. The repellent formations and the bactericidal formations.

The former refers to the bacteria-repellent property of a surface to prevent buildup or accumulation of biological materials [28]. For the second mechanism, the surface nanostructures may allow attachment by bacteria. However, they exhibit bactericidal action, destroying the adherent microbial cells, for which some authors referred them as biocidal surfaces [28]. While the eventual manifestation of either action is a significantly reduced accumulation of microorganisms and prevention of biofilm-mediated diseases without the need for any chemical agents, the underpinning mechanisms are different. Some surfaces might exhibit both actions, although the relative contribution by each action may differ.

The biophysical mechanism for killing adherent bacteria mediates through surface features of nanoscale dimensions. For example, the cicada wing has a nanopatterned with an array of 200 nm-high pillars spaced 170 nm apart, which is potently biocidal against *Pseudomonas aeruginosa*, mechanically penetrate through the cell wall and membrane within several minutes after the bacterial adhesion process began [28, 29]. Another example is the skin of gecko that shows similar biophysical antimicrobial action [30]. Replicas of the gecko skin in polymeric material also possess bactericidal effects against *Streptococcus mutans* [31], *Porphyromonas gingivalis and Escherichia coli* [32]. Many studies of the biocidal property of nanopatterned surface have used only one bacterial species for demonstration of the effect. Testing with a broader selection of clinically relevant bacterial species should provide more meaningful results. Besides, more data is needed to connect the individual design elements among the range of possible designs with their effects on bacteria. Of particular relevance to bacterial destruction by tearing, repelling and rupturing is the presence of nanotips, the aspect ratio of the protrusions and the spacings between the protrusions.

In this study, we employed a novel photolithography- based approach to fabricate biomimetic nano-structured surfaces in a PMMA material and exposed to an aqueous environment laden with three contrasting types of bacteria; round, rod-shaped and spindle shaped). Hydrated environments relate to the principle economically and medically important Specifically, this study aimed to determine the antibacterial and bactericidal effects of synthetic surface nano-protuberances with three separate height, widths and aspect ratios. These were tested against several oral bacteria morphotypes bearing slightly varying shapes, cell wall ultra-structures, wall thicknesses and interactomes. The study serves as a testbed for adapting techniques that can accurately specify protrusion dimensionality in a polymer and function against several bacteria for a niche application.

Materials and methods

2.1 Fabrication of PMMA films with surface nano-patterns of different aspect-ratios

A technique using the principle of photolithography and wet etching were used to produce a mold for casting with PMMA (Fig. 1). Briefly, a clean (111)-oriented silicon (Si) wafer with 100nm-thick surface oxide layer was coated with a photoresist, which was patterned with photolithography to obtain a regular array of square holes with a pitch of 1.5 μm (Fig. 1a). Then, the patterned surface was etched with benzoxazolinone (BOA) to remove the exposed silicon oxide layer, producing a regular array of nanoscale inversed pyramids in the Si wafer. The etching time would control the size of inversed pyramids; etching for 50 min produced the most closely packed pyramids. After removing the photoresist, the wafer was then placed in 15% tetramethylammonium hydroxide (TMAH) solution at 50°C for 50 min for wet etching (Fig. 1b). Thereafter, different thickness (400 nm, 800 nm and 1200 nm) of chromium (Cr) was sputtered on the Si wafer to form the mold (Fig. 1c). The amount of sputter coating deposited would determine the aspect ratio of the surface nano-pyramids after casting. For the casting process, PMMA solution was prepared by dissolving 10 g of PMMA powder (Alfa Aesar; Thermo Fisher Scientific, Heysham, UK) in 100 mL of toluene (Analytical

grade, RCI Labscan, Bangkok, Thailand), which solution was poured on the surface of the Cr-coated Si wafer and heat cured at 90 °C for 1 h and then 120 °C for another 30 min. A transparent PMMA film with nano-pyramids on the surface was obtained after peeling off from the mold (Fig. 1d). It was noted that the Cr happened to also serve as an anti-sticking layer such that the mold can be used many times without leaving any residues. The following groups of PMMA specimen were prepared for characterization: 1) NP400 (from a mold sputter coated with 400nm Cr); 2) NP800 (with 800nm Cr); 3) NP1200 (with 1200nm Cr); and 4) non-textured, *i.e.* smooth, flat PMMA (control group).

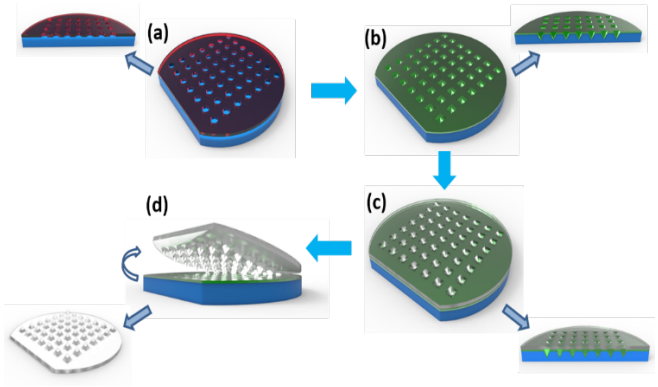

Fig. 1 - Schematics of nano-pyramidal PMMA films fabrication: (a) A <100> oriented Si wafer with 100 nm SiO_2 undergone photolithography with 1.5 µm square array pattern and BOA etching; (b) the patterned wafer undergone TMAH etching to form i-pyramid template; (c) different thickness of chromium sputtered on the surface; (d) regular nanopyramid on PMMA film after peeling off.

2.2 Characterization

Roughness values (Ra) were obtained using an AFM (Dimension edge with ScanAsyst™; Bruker, Santa Barbara, CA, USA), and the calculations for surface roughness and micro-hardness were carried out using the supplied software (NanoScope Analysis 1.5; Bruker, Santa Barbara). Furthermore, static water contact angle (WCA) value and the surface free energy (SFE) were measured by a contact angle goniometer (SL200KB; KINO, Norcross, GA, USA) and estimated in software (CAST3.0; KINO, Norcross). All specimens were then affixed on copper holders, sputter-coated with gold using a magnetron sputtering deposition system (Dynavac CS300, Hingham, MA, USA) for 100 s. and examined in a field-emission scanning electron microscope (JSM-7800F; JOEL, Peabody, MA, USA) operating at 5 kV. High-resolution micrographs of the topographical features were taken at different magnifications (×5,000, ×10,000 and ×20,000).

2.3 Biofilm cultivation and examination

Four representative pathogenic bacteria were selected for use in this study: a cariogenic gram-positive, facultative anaerobic bacterium, *S. mutans* (ATCC 33277; American Type Culture Collection, Manassas, VA, USA); a gram-positive facultative anaerobic bacterium, *E. faecalis* (ATCC 29212); a gram-negative, strictly anaerobic periodontal pathogen, *P. gingivalis* (ATCC 35668); and a gram-negative anaerobic spindle-shaped bacterium, *F. nucleatum* (ATCC 25586). *E. faecalis* and *F. nucleatum* were frequently isolated from root canal failures, whereas *S. mutans* and *P. gingivalis* from the tooth and root surfaces, respectively. Prior to the experiment, each species of bacteria was inoculated on blood agar plate and cultured anaerobically for 24 h. Then, a scoop of bacteria was taken from one colony and transferred into a sterile broth for preparing a bacterial suspension. *S. mutans* and *E. faecalis* were added to brain heart infusion (BHI) broth (Oxoid™, Thermo Fisher Scientific, Basingstoke, Hampshire, UK), whereas *P. gingivalis* and *F. nucleatum* were cultured in a broth containing (in 1 L) 30 g tryptic soy broth (TSB) (Difco; Becton Dickinson, Franklin Lakes, NJ, USA), 5 g yeast extract (Difco) and 10 mL hemin (Sigma-Aldrich; St. Louis, MO, USA). The suspensions were titrated to OD660 = 0.500–0.517 with a spectrophotometer (DU® 730 Life Science UV/Vis Spectrophotometer; Beckman Coulter, Brea, CA, USA), which corresponded to a concentration of 1.0×10^9 CFU/mL (McFarland standard 4). Segments of PMMA films (size 0.5 cm × 0.5 cm, n=3 for each group) were sterilized using 4% Clorox before use for 10 min, and rinsed with sterilized distilled water for 1 min. The PMMA samples were placed, with the nano-patterned surface facing upward to allow bacterial adhesion, inside individual culture wells of a sterile 24-well culture plate (Corning Glass Works, New York, USA), into which 1 mL bacterial suspension was added into each. Aseptic technique was strictly followed. All samples were then incubated anaerobically (atmosphere N_2:CO_2:H_2 = 8:1:1 by volume) at 37 °C for 1 h, 24 h, 72 h or 168 h, before microscopic examinations. The broth was replaced daily during the incubation period.

2.4 Microscopic examinations

Two microscopic methods were employed to examine the bacterial vitality, distribution, morphology, adhesion, and subsequently calculate and determine the killing/impairing efficiency for each surface. First, each specimen was stained using a LIVE/DEAD BacLight™ Bacterial Viability Kit (L7012 Invitrogen; Molecular Probes, Eugene, OR, USA) in the dark at room temperature for 30 min. The growth of bacteria was calculated for each specimen from the green and red fluorescence signal (representing live and dead bacterial cells, respectively) via a confocal laser scanning microscope (CLSM) (IX81 FluoView FV1000; Olympus, Shinjuku-ku, Tokyo, Japan). Six independent and randomly selected areas were imaged from each specimen. All CLSM images were imported into the computer, and the amount of live and dead bacterial cells in every observation field were determined using an image analysis software (ImageJ; National Institutes of Health, Bethesda, Maryland, USA). All quantitative data were analysed in a statistical software (SPSS 11.0; SPSS Inc., Chicago, IL, USA).

After CLSM examination, the specimens were retrieved and fixed in 2.5% glutaraldehyde solution for 1 h. Then, they were serially dehydrated by increasing concentrations of ethanol, from 70% up to 100%. The samples were then inspected in a field-emission scanning electron microscope (JSM-7800F) operating at 5 kV. High-resolution micrographs of the nano-pattern and the morphological appearance of the bacterial cells on each surface were taken at different magnifications (×5,000, ×10,000 and ×20,000).

1. Results

3.1 Characterization of nano-patterned surface

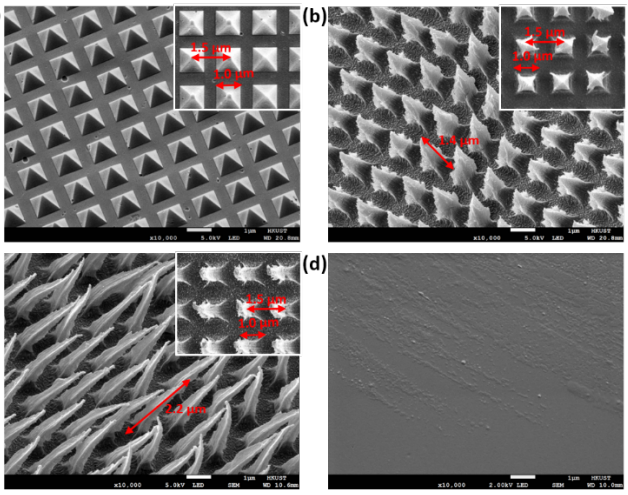

Group	Periodicity (µm)	Spacing (nm)	Height (µm)	Width (µm)	Aspect ratio
NP400	1.5	500	1.0	1.0	1.0
NP800	1.5	500	1.4	1.0	1.4
NP1200	1.5	500	2.2	1.0	2.2

Fig. 2 - SEM micrographs showing the topographies of the different nano-patterned PMMA surfaces: (a) NP400, (b) NP800, (c) NP1200, (d) smooth control; and (e) the measured parameters of the surface PMMA nano-features. (Scale bar = 1 µm, magnification: ×10,000)

Nanoscale pyramidal protrusions on the PMMA surface were observed in all groups (Fig. 2). Group NP400 showed low-rise, square based, nanoscale pyramids with an aspect ratio of 1 (Fig. 2a). The spinules/nanospikes in group NP800 were taller, at about 2 µm, with an aspect ratio of about 1.4 and with a more definite pointed tip (Fig. 2b). The NP1200 group showed slender spinules of about 3 µm tall, with pointed tips and an aspect ratio greater than 2 (Fig. 2c). Some variations in the spinule height of group NP800 and NP1200 were noted. The periodicity, or the distance between the centers of the nano-pyramidal base of each spinule, was measured to be 1.5 µm – that distance being the same as was specified for the photolithographic equipment. By deduction, the distance between the base of each nanopyramid and its neighbors was 500 nanometers.

Group	WCA (deg)	SFE (J/m²)	Drop profile
Control	78.68 ± 0.00	35.20 ± 0.04	
NP400	88.59 ± 0.20	29.08 ± 0.12	
NP800	111.27 ± 0.16	15.62 ± 0.09	
NP1200	93.63 ± 0.20	26.00 ± 0.12	

Tab. 1 - Static water contact angle (WCA) and calculated surface free energy (SFE) for each group.

The Ra value of the nano-patterned surfaces was 43.7 ± 2.65 nm for NP400, 53.1 ± 8.78 nm (for NP800), and 108.0 ± 13.4 nm for NP1200 group. All of them were statistically different from that of the smooth control (15.9 ± 2.9 nm) (p<0.05). The static WCA values increased significantly from 78.68° (control) to about 90° for NP400, or greater (111.27 ± 0.16° for NP800; 93.63 ± 0.20° for NP1200) – the corresponding SFE values of all nano-patterned surfaces tested were significantly lower than the control group (Tab. 1). The NP800 group was noted to have the greatest contact angle, with the lowest free surface energy.

3.2 Bacterial viability and adhesion

3.2.1 Streptococcus mutans

CLSM examination showed significant reduction in amounts of live *S. mutans* cells, but increase in dead ones, either in absolute amount or in terms of proportion, at the various timepoints throughout the incubation period, when compared to the control group (Fig. 3).

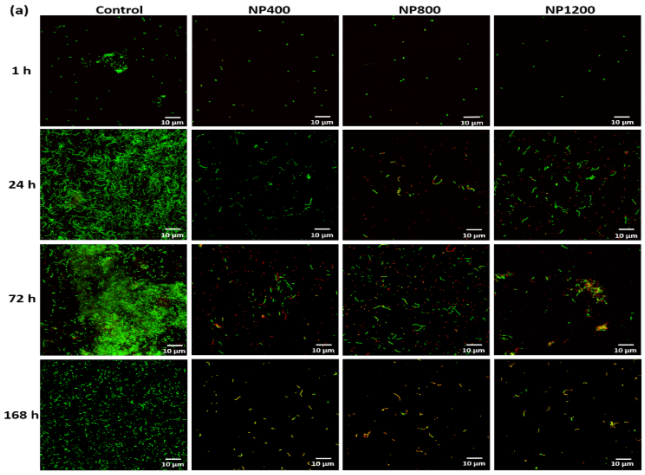

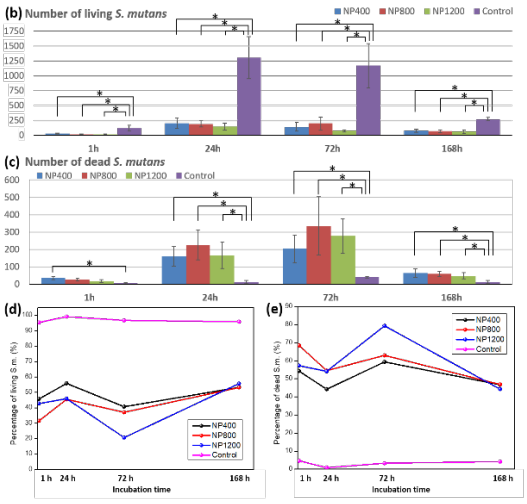

Fig. 3 - Viability of *S. mutans* on the different surfaces at the different incubation time: (a) CLSM images of live (green) and dead (red) bacterial cells; (b) number of live *S. mutans*, (c) number of dead *S. mutans*, (d) percentage of live *S. mutans*, (e) percentage of dead *S. mutans* (measurement area = 126 × 126 μm², image size = 640 × 640 pixels) (Error bars = 95% CI, *p<0.05)

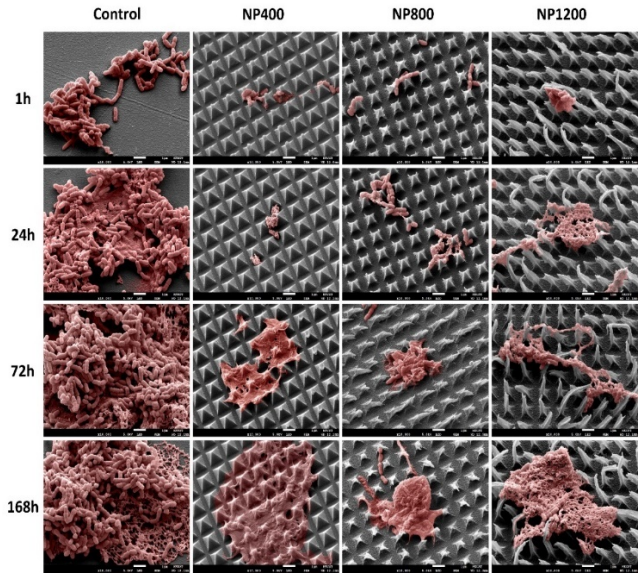

Fig. 4 - SEM images of *S. mutans* (colored in pink in the image manipulation software (Photoshop CS6; Adobe, USA)) on different PMMA surfaces after different periods of incubation (Scale bar = 1 μm, magnification: ×10,000)

The SEM appearance of the bacterial aggregates of the control group was in stark contrast to those on the nano-patterned surfaces (Fig. 4). Bacterial cells gathered on the smooth PMMA surface of the control group, which became denser and thicker at longer incubation periods. The outline of individual cells could be identified. In contrast, *S. mutans* failed to congregate into any form of organized mass on all experimental groups. Instead, the bacterial cells were found only in very small clusters. After 1 day of incubation, all experimental groups with nano-patterned surface, despite the different aspect ratios of their nanostructure, showed an apparently high degree of biofilm repellency, with the bacterial cells remaining isolated or only gathering in tiny aggregates. Where clusters of *S. mutans* were found, they often were situated in between, and some near the pointed tips of, the nano-spinules. The appearance was similar after 3 days to 1 week of incubation – the nano-patterned surfaces remained with little sign of biofilm formation or with the biofilm severely disrupted. For those (small) areas with accumulation of *S. mutans*, the colonies looked very different from that of the control group and they appeared very thin, with the outline of individual cells being either blur or unidentifiable. There nano-spinules of the NP1200 groups appeared flexible.

3.2.2 *Enterococcus faecalis*

For the experimental nano-patterned groups, *E. faecalis* demonstrated a very similar trend of significant reduction in live bacterial cells, but increase in dead ones, at the various timepoints throughout the incubation period (Fig. 5). The proportion of live cells dropped to an apparent minimum after 3 days, and gradually return at 1 week, although the total amount of bacteria remained significantly lower than the control.

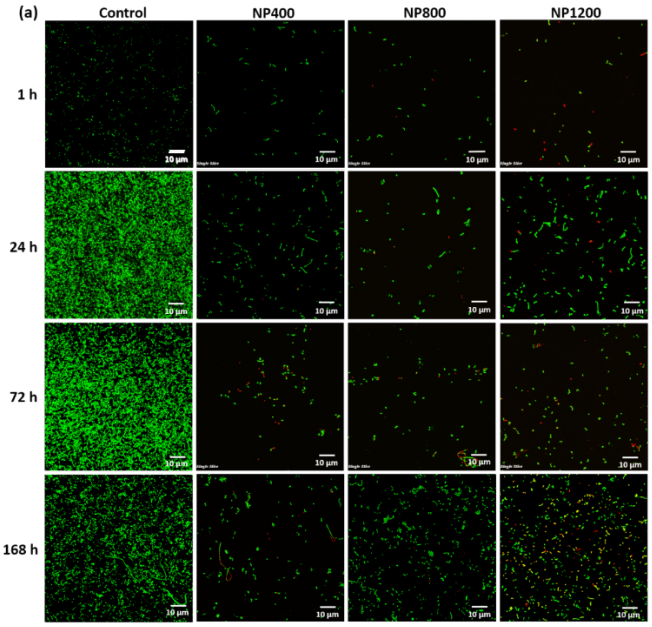

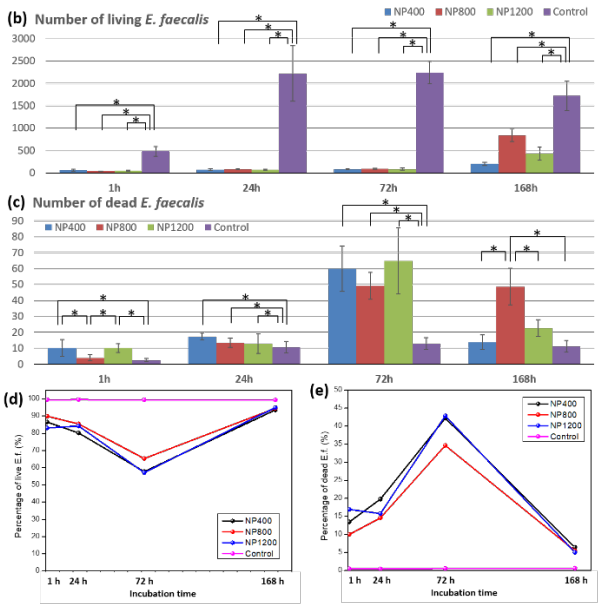

Fig. 5 - Viability of *E. faecalis* on the different surfaces at the different incubation time: (a) CLSM images of live (green) and dead (red) bacterial cells; (b) number of live *E. faecalis*, (c) number of dead *E. faecalis*, (d) percentage of live *E. faecalis*, (e) percentage of

dead *E. faecalis* (measurement area = 126 × 126 μm², image size = 640 × 640 pixels) (Error bars = 95% CI, *p<0.05)

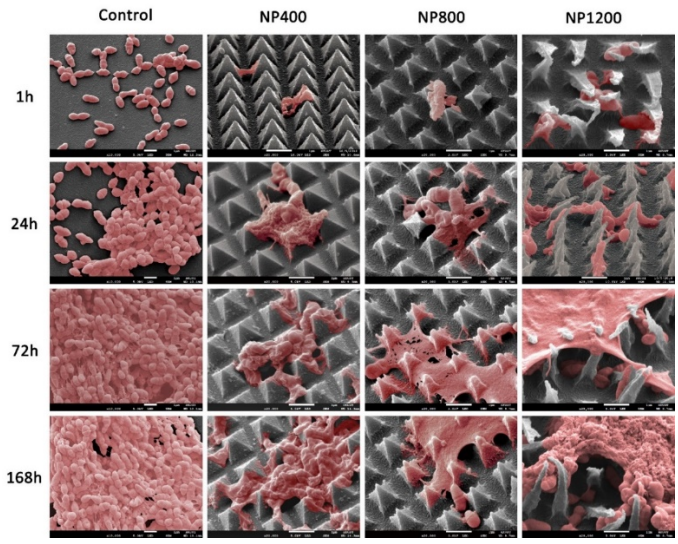

Fig. 6 - SEM images of *E. faecalis* (colored in pink in the image manipulation software Photoshop CS6) on different PMMA surfaces after different periods of incubation. (Scale bar = 1 μm, magnification: ×10,000)

Similar to the observations for *S. mutans*, there were stark differences in the colonization of *E. faecalis* on the nano-patterned surfaces versus the smooth PMMA surface (Fig. 6). At 1-hour post-incubation, some isolated bacterial cells were either "trapped" in between the nano-spinules, or situated at or close to the tips, while bacterial cells were clustering on the smooth control surface. After 1 day of incubation, thick aggregates of *E. faecalis* cells and some extracellular materials were present and covering a large part of the smooth surface; similar appearance was observed after 3 days or 1 week in the control group. In contrast, there were some tiny clusters of bacteria dispersed in between the nano-protrusions; some other cells were situated on top of the spinules. The outline of individual bacterial cells was not clear. At 72 hours and 1 week after incubation, a form of biofilm-like structure was frequently seen on the nano-patterned groups. All of them seemed to have been disturbed/disrupted to an extent that no individual cells could be identified. The pointed tips of the nano-spinules were seen to have "pierced" through the film-like structures, especially in the NP800 and NP1200 group. Some bacterial cells appeared stuck between the nano-protrusions.

1.2.3 Porphyromonas gingivalis

Similar trends were observed for samples cultured with *P. gingivalis* (Fig. 7). CLSM examination revealed remarkable differences in bacterial growth between the smooth control and the nano-patterned surfaces (Fig. 7a). The differences between experimental groups were relatively small. Generally, for the experimental groups, the proportion of living bacteria kept decreasing from around 85% to about 35% (NP800) to 50% (NP400 and NP1200), whereas that of the control group remained quite stable at just below 100% throughout the incubation period (Fig. 7d). The proportion of dead bacteria went up dramatically for the experimental groups, whereas the figure was just above 0% for the control throughout (Fig. 7e). The overall amounts of bacteria residing on the nano-patterned surfaces were significantly lower than the smooth control surface (p<0.05).

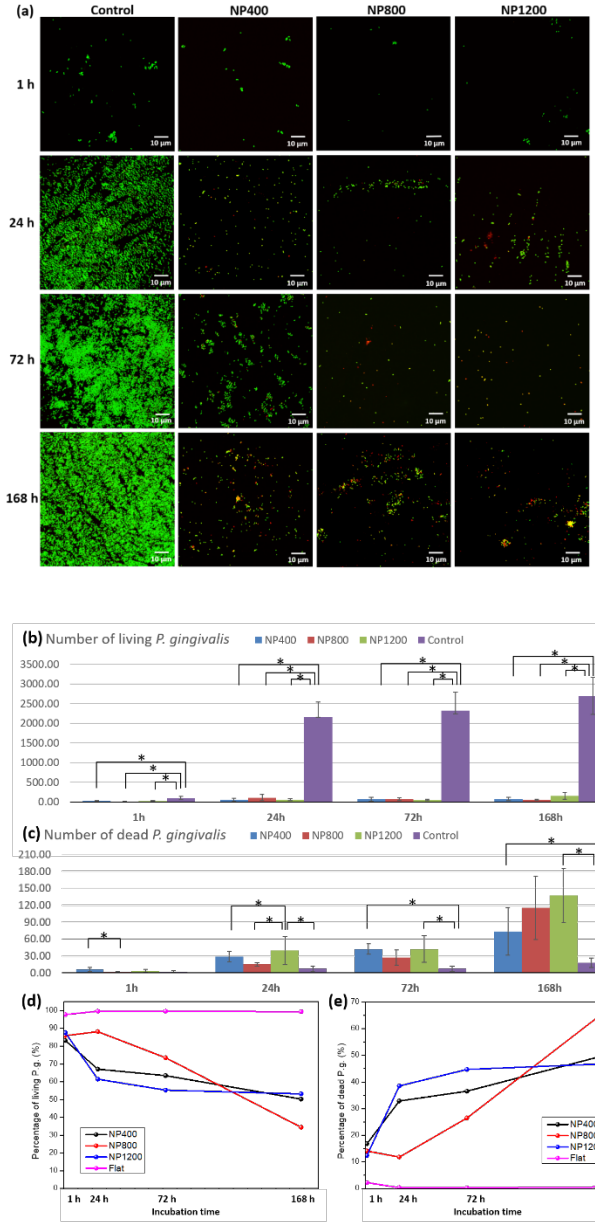

Fig. 7 - Viability of *P. gingivalis* on the different surfaces at the different incubation time: (a) CLSM images of live (green) and dead (red) bacterial cells; (b) number of live *P. gingivalis*, (c) number of dead *P. gingivalis*, (d) percentage of live *P. gingivalis*, (e) percentage of dead *P. gingivalis* (measurement area = 126 × 126 μm², image size = 640 × 640 pixels) (Error bars = 95% CI, *p<0.05)

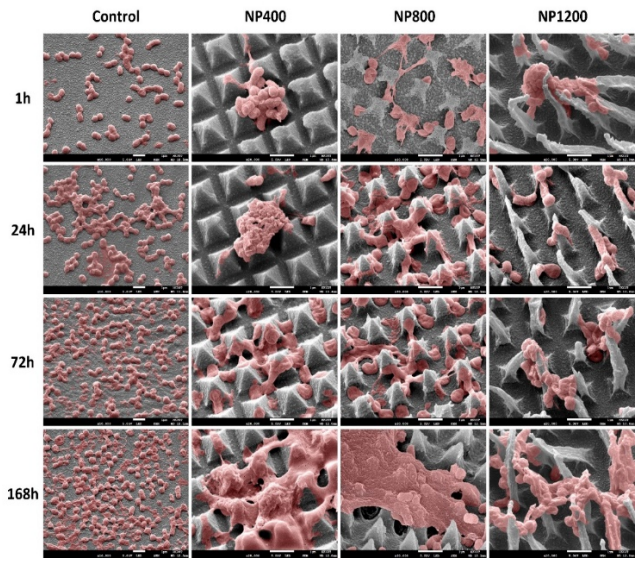

Fig. 8 - SEM images of *P. gingivalis* (colored in pink in the image manipulation software Photoshop CS6) on different PMMA surfaces after different periods of incubation. (Scale bar = 1 µm, magnification: ×10,000)

For this slow-growing species, generally there were fewer *P. gingivalis* cells residing on the smooth surface of the control group; their number increased over time and formed thin aggregates. There were plenty of cell-to-cell contacts, but the outline of individual cells remained identifiable (Fig. 8). For the nano-patterned PMMA surfaces, at 1 hour, few bacterial cells were seen among the nanoscale protrusions. After 1 day of incubation, more cells were present in a very disordered manner, some of which were mounting on the tips, but the majority were lodged in the spaces in between the nano-spinules. The appearance was similar at 3 days post-incubation, with the bacterial cells situated mostly in between the spinules and with little sign of biofilm formation. After 1 week, some areas with biofilm-like structure were observed, but no identifiable cell outline could be noticed. The film-like structures appeared to have been punctured by the nano-protrusions, especially in the NP800 and NP1200 group. Evidence of disrupted bacterial accumulation could be observed.

3.2.4 Fusobacterium nucleatum

CLSM examination revealed a similar trend of the amount of *F. nucleatum* as with other bacterial species tested. The amount was significantly reduced on the nanopatterned surfaces at all incubation periods (p<0.05). However, the difference in the number of live bacteria between experimental groups was not statistically significant (Fig. 9).

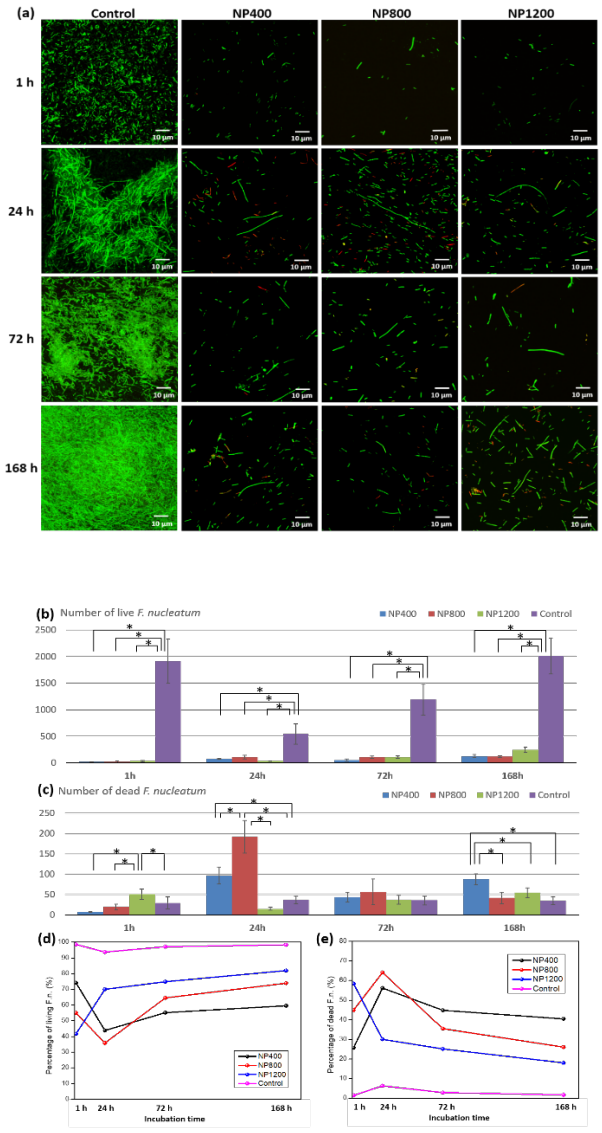

Fig. 9 - Viability of *F. nucleatum* on the different surfaces at the different incubation time: (a) CLSM images of live (green) and dead (red) *F. nucleatum*; (b) number of live *F. nucleatum*, (c) number of dead *F. nucleatum*, (d) percentage of live *F. nucleatum*, (e) percentage of dead *F. nucleatum* (measurement area = 126 × 126 µm^2, image size = 640 × 640 pixels). (Error bars = 95% CI, *p<0.05)

SEM examination revealed that packing of these filamentous bacteria was obviously less dense on the nano-patterned surfaces, compared with the smooth control (Fig. 10). While the bacterial mass became denser and thicker on the smooth surface in time, large areas of uncolonized region were observed for the experimental groups. During the incubation period from 1 day to 1 week, some bacterial cells that were present at the tips of the nano-spinules seemed to have been ruptured, with the cell outline becoming shrunken, irregular and poorly defined, when compared with those in the control group (Fig. 10). Some filamentous cells were lodged in the valleys in between the nano-protrusions with part of the cell outline seemingly stretched and some parts shrunken.

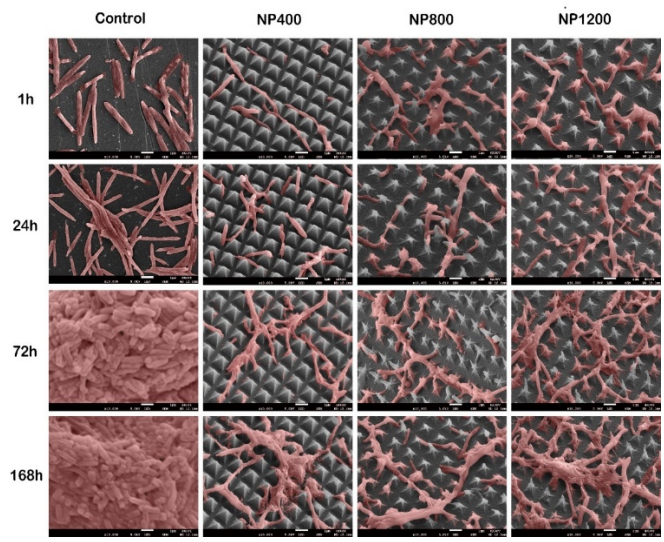

Fig. 10 - SEM images of *F. nucleatum* (colored in pink in the image manipulation software Photoshop CS6) on different PMMA surfaces from 1 hour to 1 week. (Scale bar = 1 µm, magnification: ×10,000)

2. Discussion

Photolithography is a fabrication process that can produce precise surface nanostructures at very high resolution. It is versatile and requires very little post-fabrication sample preparations [33; Tsui 2018]. Various patterns of different aspect ratio are possible using this fabrication method. By controlling the amount of chromium deposition, it is possible to control the aspect ratio of the nanoscale protrusions, for optimization of the parameters to achieve the best result with respect to bacterial attachment and settlement. There were some variations in the measured height of NP800 and NP1200 spinules, possibly due to stretching and deformation during peeling from the mold. Those "long" spinules of NP1200 group appears somewhat flexible, but that did not seem to have affect the bactericidal property of that surface. Mathematically, nanoscale protrusions with higher density or aspect ratio could lead to greater stretching of the cell membrane and hence rupturing of the bacterial cell, as a result of an increase in contact area [31; Li X, 2016].

Bacterial attachment and biofilm formation are sophisticated processes. The physical interaction between bacterial cells and surface topography is an intricate process. Not only are the size and shape of the bacterial cell, its membrane rigidity and the presence of membrane features involved in mobility, sensing and anchorage to a surface [29; Feng 2015], but also the ability of bacteria to form cell-cell connections would also affect their response to any topographical features [28; Anselme 2010]. Thus, difference in behavior should be expected among different species [32; Perera-Costa 2014]. For that reason, this in vitro study tested the various nano-patterned surfaces using several representative and pathogenic species of the oral microflora. It has been reported that the number of bacterial cells (*S. aureus*, *P. aeruginosa* and *E. coli*) and of extracellular polysaccharide (EPS) attaching to a titanium surface were inversely related to the average roughness (Ra) value [7; Han 2018, 38; Teughels 2016, 39; Quirynen 1993]. Similar result was reported for glass, such that smooth glass surface with a Ra value of 1.3 nm mediated more attachment of eight different bacterial species than glass surface of Ra = 2.1 nm [29; Feng 2015]. The Ra values of the nano-patterned surfaces increased with the aspect ratio of the nano-pyramids, a phenomenon that is expected. The present results suggested that PMMA with nanoscale pyramidal projections possess both antibiofouling and bactericidal effects against the four species of oral bacteria tested. Subjectively, the longer spinules (*i.e.* NP800 and NP1200 group) were more often seen to penetrate through biofilm-like structure, whereas bacterial cells were frequently seen to be trapped among nano-protrusions of a lower aspect ratio as in the NP400 group. Further study for the optimal Ra, or aspect ratio, for the nano-protrusions is warranted.

Bacteria and cells are keen to adapt to non-native environments, with attempt to spread over and adhere to the surface. When the bacterial cells encounter an array of nanopillar nanostructure, their cell wall would be in contact with multiple pillars, leading to distortions of the cell wall at the interface and the resultant stresses would lead to the rupture of the cell [40, 41; Turner 2013/ Aguado 2012]. Bacteria that actively bind to a surface might be more susceptible to such mechanism of death by physical damage [42; Watson, 2019]. The free surface energy and spacing between nanopillars have been suggested as important factors that favor the stretching of the bacterial wall, leading to ultimate cell death. A higher death rate of bacteria was proposed for narrower spacing for the nanoscale protrusions [42; Watson, 2019]. Although a fixed spacing (of 500 nm) between the nano-spinules was employed in the making of the nano-patterned surface in this study, the influence of that spacing would benefit from further experimentation to optimize this particular parameter against the pathogenic microorganisms in the mouth.

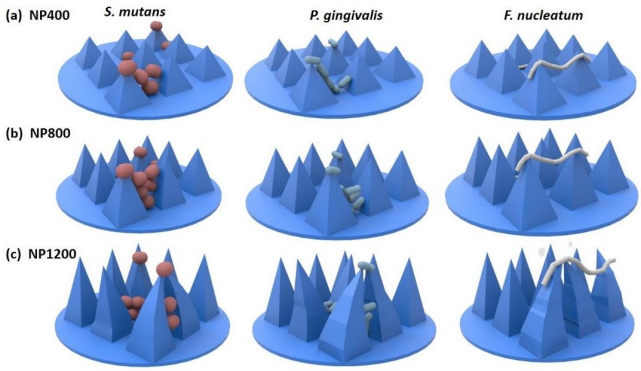

Fig. 11 - Hypothesised mechanisms for bacterial cell death by tearing, rupture, and puncturing. The nano-patterned pyramidal protrusions cause the damage. Bacteria are set-up to interact with the nanoscale structures of different height, width, and aspect ratio: categorized into three test groups (a) NP400, (b) NP800, and (c) NP1200.

We propose a series of mechanisms for the rupturing of bacteria by the pyramid tips- pictured in Fig. 12. In brief, bacterial cells make multiple physical contacts to the sides of the nano-protrusions. *F. nucleatum* extends fimbrae to facilitate attachment to the complex topography. Protrusion spacings that are slightly larger than the cells, but at distances sufficient to allow contacts with the pyramid edge, caused the bacteria to stretch themselves, to compress, and to have their cell wall punctured. We can see snapshots of the physical

damage in SEM images of the bacteria covered surfaces. The larger (10 microns) bacterial cells by length extende (*F. nucleatum*) is therefore 20 x larger than the spacing of 0.5 μm, ruptured in SEM and killed as a result of penetration from the pyramid apices (Fig. 12). Although, a fraction of *F. nucleatum* cells aligned themselves between the pyramidal apices because the bacterial width (0.4-0.7 μm) fits between the pyramids. In this case, they are liable to rupture by overstretching as they attempt to make enough contacts for stable support and attachment. For the smaller cells than *F. nucleatum (10 μm)*, include *P. gingivalis* (0.3~0.5 μm), *S. mutans*, and *E. faecalis* (0.5~1μm), they descended between the nanopyramids. By this logic, if the spacing of the arrays decreased, the smaller cells are more easily punctured and die. This simple mechanistic model for the death of bacterial cells on contact with different spaced pyramids correlates with CLSM and SEM snapshots of bacteria on the various pyramid arrangements.

We fabricated PMMA materials with antibacterial textures against a broad range of dental pathogens. PMMA is a biomaterial with high utility in ophthalmology, dentistry and orthopaedics and as a general material for preventing microbial contamination and disease transmission in hospital environments. Specifically, the data on oral pathogens highlights the utility for making removable partial and complete dentures. Prostheses of this kind are often provided to the elderly or compromised individuals who may present less-than-optimal oral hygiene; the accumulation of years of wear and tear. Further study is to characterize the responses of more types of bacteria, pathogens and benign species differing in size, morphology, mobility, and aggregation. In doing so, we broaden the functional reach of the pyramid motif, which can be readily inscribed into every selected material, polymers, ceramics and particularly polymers.

3. Conclusions

Nano-patterned surfaces serialized with varying dimensions of nanoscale protrusions were fabricated into the surface of PMMA = and evaluated for their effectiveness against several oral pathogens to illustrate application for a particular medical niche; and could well adapt to other ophthalmological, endothelial niche. These selected pathogens comprised of bacterial species with multivariate shape (three shapes: cocci/rod and fusiform rods of spindle), three sizes (0.5–0.75 μm/ 0.5-1.2 μm/0.4-10 μm), three capsule structures (gram negative and gram positive) and architectural design. In all three examples, the nano-patterned PMMA surfaces showed high levels of damage against contacting bacteria leading to death rates of up to 80%. Materials textured with gecko-inspired protrusions possess great utility on film surface for medical implants, medical devices and

Conflicts of interest

There are no conflicts to declare.

Acknowledgements

This work was supported by the National Natural Science Foundation of China (Grant No.: 81901058), Hong Kong Innovation and Technology Fund (ITS/362/14FP and ITS/415/16) of the Innovation and Technology Commission of HKSAR, the Endodontic Research Fund of the Faculty of Dentistry, the University of Hong Kong (Account No.: 102009653.012058.08008.310) and the General Research Fund (project 16237816) of the Hong Kong Research Grant Council. We also thank the Nanosystem Fabrication Facility (NFF) of HKUST for helping with the nanofabrication.

Notes and references

[1] B. Schachter, *Nat Biotechnol*, 2003, **21**, 361
[2] A.F. Han, J.K.H. Tsoi, F.P. Rodrigues, J.G. Leprince, W.M. Palin. *Int J Adhe Adhe*, 2016, **69**, 58.
[3] C.M. Tan, J.K.H Tsoi, C.J. Seneviratne, J.P. Matinlinna. *J Prosthodont Res*, 2014, **58**, 243.
[4] A. Han, J.K.H Tsoi, J.P. Matinlinna, Y. Zhang, Z. Chen. *Dent Mater*, 2018, **34**, 272.
[5] P.A. Slullitel, M.A. Buttaro, G. Greco, J.I. Onativia, M.L. Sanchez, S. Mc Loughlin, C. Garcia-Avila, F. Comba, G.F. Zanotti, F. Piccaluga, *Orthop Traumatol Surg Res*, 2018, **104**, 439.
[6] H. van de Belt, D. Neut, W. Schenk, J.R. van Horn, H.C. van der Mei, H.J. Busscher. *Biomaterials*, 2001, **22**, 1607.
[7] E.B. Minelli, T. Della Bora, A. Benini, *Anaerobe*, 2011, **17**, 380.
[8] P.J.M. Bispo, W. Haas, M.S. Gilmore, *Pathogens*, 2015, **4**, 111.
[9] D. J. Stickler, *Nat Clin Pract Urol,* 2008, **5**, 598.
[10] R.Q. Frazer, R.T. Byron, P.B. Osborne, K.P. West, *J Long Term Eff Med Implants*, 2005, **15**, 629.
[11] M. Katsikogianni, Y.F. Missirlis, *Eur Cells Mater*, 2004, **8**, 37.
[12] C. Sahin, A. Ergin, S. Ayyildiz, E. Cosgun, G. Uzun, *J Adv Prosthodont*, 2013, **5**, 140.
[13] I. Olsen, M.A. Taubman, S.K. Singhrao, *J Oral Microbiol*, 2016, **8**, 33029.
[15] A.K. Epstein, B. Pokroy, A. Seminara, J. Aizenberg. *P Natl Acad Sci USA*, 2011, **108**, 995.
[16] R.J. Fair, Y. Tor, *Perspect Medicin Chem*, 2014, **6**, 25.
[17] H. Mortazavi, M. Baharvand, M. Mehdipour, *J Dent Res Dent Clin Dent Prospects*, 2014, **8**, 6.
[18] D. McShan, P.C. Ray, H. Yu, *J Food Drug Anal*, 2014, **22**, 116.
[19] M.R. Anaraki, A. Jangjoo, F. Alimoradi, S.M. Dizaj, L. Farzaneh, *Pharm Sci*, 2017, **23**, 207.
[20] C.M. Tan, J.K. Tsoi, C.J. Seneviratne, J.P. Matinlinna, *J Prosthodont Res*, 2014, **58**, 243.
[21] A.F. Han, X.L. Li, B.X. Huang, J.K.H. Tsoi, J.P. Matinlinna, Z.F. Chen, D.M. Deng, *Int J Adhes Adhes*, 2016, **69**, 125.
[22] S.M. Kelleher, O. Habimana, J. Lawler, B. O' Reilly, S. Daniels, E. Casey, A. Cowley, *ACS Appl Mater Interfaces*, 2016, **8**, 14966.
[23] K. Anselme, P. Davidson, A.M. Popa, M. Giazzon, M. Liley, L. Ploux, *Acta Biomater*, 2010, **6**, 3824.
[24] G.P. Feng, Y.F. Cheng, S. Wang, D.A. Borca-Tasciuc, R.W. Worobo, C.I. Moraru, *Nature Partner Journals Biofilms and Microbiomes*, 2015, **1**, 9.
[25] J. Hasan, H.K. Webb, V.K. Truong, S. Pogodin, V.A. Baulin, G.S. Watson, J.A. Watson, R.J. Crawford, E.P. Ivanova, *Appl Microbiol Biotechnol,* 2013, **97**, 9257.
[26] X. Li, Bactericidal mechanism of nanopatterned surfaces. *Phys Chem Chem Phys*, 2016, **18**, 1311.
[27] D. Perera-Costa, J.M. Bruque, M.L. Gonzalez-Martin, A.C. Gomez-Garcia, V. Vadillo-Rodriguez, *Langmuir*, 2014, **30**, 4633.

[28] E.P. Ivanova, J. Hasan, H.K. Webb, V.K. Truong, G.S. Watson, J.A. Watson, V.A. Baulin, S. Pogodin, J.Y. Wang, M.J. Tobin, C. Lobbe, R.J. Crawford, *Small*, 2012, **8**, 2489.
[29] G.S. Watson, D.W. Green, M. Sun, A. Liang, X. Li, B.W. Cribb, J.A. Watso, *J NanoSci Adv Tech*, 2015, **1**, 1.
[30] G.S. Watson, D.W. Green, L. Schwarzkopf, X. Li, B.W. Cribb, S. Myhra, J.A. Watson, *Acta biomater*, 2015, **21**, 119.
[31] X. Li, G.S.P Cheung, G.W. Watson, J.A. Watson, S. Lin, L. Schwarzkopf, D.W. Green, *Nanoscale*, 2016, **8**, 18860.
[32] K.H. Tsui, X. Li, J.K.H. Tsoi, S.F. Leung, L. Tang, W.Y. Chak, C. Zhang, J. Chen, G.S.P. Cheung, Z. Fan, *Nanoscale*, 2018,
2, **10**, 10436.
[33] W. Teughels, N. Van Assche, I. Sliepen, M. Quirynen, *Clin Oral Implants Res*, 2006, **17**, 68.
[34] M. Quirynen, H.C. van der Mei, C.M. Bollen, A. Schotte, M. Marechal, G.I. Doornbusch, I. Naert, H.J. Busscher, D. van Steenberghe, *J Dent Res*, 1993, **72**, 1304.
[35] R.D. Turner, A.F. Hurd, A. Cadby, J.K. Hobbs, S.J. Foster, *Nat Commun*, 2013, **4**, 1496.
[36] B.A. Aguado, W. Mulyasasmita, J. Su, K.J. Lampe, S.C. Heilshorn, *Tissue Eng*, 2012, **18**, 806.
[37] G.S. Watson, D.W. Green, J.A. Watson, Z. Zhou, X. Li, G.S.P. Cheung, M. Gellender, *Adv Mater Interfaces*, 2019, **6**, 1801646.

